JOURNAL OF AIRCRAFT
Vol. 37, No. 5, September–October 2000

Numerical Study on Reduction of Transonic Blade-Vortex Interaction Noise

San-Yih Lin,* Yan-Shin Chin,† and Bae-Yih Hwang‡
National Cheng-Kung University, Tainan 70101, Taiwan, Republic of China

Reduction of noise caused by transonic blade-vortex interaction (BVI) is investigated numerically. The near and midfield flowfields are obtained by an Euler solver. The Euler solver is based on a third-order upwind finite volume scheme in space and a second-order explicit Runge–Kutta scheme in time. Far-field noise is then obtained from the Kirchhoff method. Two control techniques, blowing/suction and porous wall on the airfoil surface, are investigated to reduce two dominant disturbances, transonic and compressibility waves, in the BVI noise signature. Numerical results indicate that the blowing/suction control technique reduces the fluctuations generated by the transonic wave but has little influence on the compressibility wave unless it is employed at the leading edge of the blade. With surface porosity control both compressibility and transonic waves are satisfactorily reduced.

I. Introduction

IMPULSIVE noise of the blade-vortex interaction (BVI) is one of the important noise sources for helicopters. Many experimental, numerical, and theoretical studies have been carried out to investigate the mechanisms and dominant factors of BVI noise.[1–4] For a review of helicopter impulsive noise, please see Schmitz and Yu.[1] George and Lyrintzis[2] used the VTRAN2 code and Kirchhoff method to study the midfield and far-field noise generated by transonic BVI. They identified numerically two dominated BVI waves, compressibility and transonic waves for the first time, and found that the far-field radiation is affected by Mach number, airfoil thickness, shape, and vortex miss distance. Lee et al.[3] pointed out that "the main source mechanism of BVI noise is the formation of an acoustic dipole (pressure fluctuation) near the leading edge, which is caused by the transition of stagnation point and suction peak." Moreover, Lent et al.[4] observed experimentally that there are two dominant sound waves, compressibility and transonic waves. Lin and Chin[5] have studied numerically the transition of stagnation point, the shock motions, and these two dominant sound waves in detailed. Here we apply an Euler solver, MOC scheme,[5,6] to study this subject. Far-field noise is then obtained using the Kirchhoff method.[7]

Flow control has long been applied to remedy unwanted phenomena in aerodynamics. In this paper we plan to control the noise radiation from BVI. Instead of directly eliminating noise in the flowfield, we attempt to reduce the noise source strength. Two control techniques, blowing/suction and porous wall on the airfoil surface, are investigated. Hartwich[8] has performed study on porous transonic airfoils by using an Euler solver. Lee[9] studied the effects of leading-edge porosity on BVI noise. In this paper, for the blowing/suction technique, an active control law according to the lift coefficient is proposed and, for the porous wall technique, two positions of the porous cavity on the airfoil surface are selected for comparison on the reduction of BVI noise. The numerical Euler solver and Kirchhoff method are introduced in Sec. II. Numerical tests are presented in Sec. III. In Sec. IV the blowing/suction technique is discussed. The effect of porosity on airfoil surface is explored in Sec. V.

Received 2 May 1998; revision received 5 April 2000; accepted for publication 7 April 2000.

*Professor, Institute of Aeronautics and Astronautics. Member AIAA.
†Associate Professor, General Education Center, The Overseas Chinese Institute of Technology, Taichung 40101, Taiwan, Republic of China.
‡Graduate Student, Institute of Aeronautics and Astronautics.

II. Computational Methods

The near and midfield flowfields of the transonic BVI are obtained by an Euler solver. The Euler solver is based on a third-order upwind finite volume scheme in space and a second-order explicit Runge–Kutta scheme in time. Far-field noise is then obtained using the Kirchhoff method.

A. Euler Solver, Modified Osher–Chakravarthy Scheme

Flows of two-dimensional, compressible, inviscid, and non-heat-conducting fluid can be described in conservation form by the Euler equations:

$$W_t + F_x + G_y = 0 \tag{1}$$

where

$$W = \begin{pmatrix} \rho \\ \rho u \\ \rho v \\ \rho e \end{pmatrix}, \qquad F = \begin{pmatrix} \rho u \\ \rho u^2 + p \\ \rho uv \\ u(\rho e + p) \end{pmatrix}, \qquad G = \begin{pmatrix} \rho v \\ \rho uv \\ \rho v^2 + p \\ v(\rho e + p) \end{pmatrix}$$

Here p, ρ, u, v, and e are the pressure, density, x- and y-directional velocity components, and the total energy per unit mass, respectively. The pressure p is given by the equation of state for a perfect gas:

$$p = (\gamma - 1)\left[\rho e - \tfrac{1}{2}\rho(u^2 + v^2)\right]$$

where γ (= 1.4 for air) is the ratio of specific heats.

The Euler solver [modified Osher–Chakravarthy scheme (MOC) scheme[5,6]] solves the two-dimensional, unsteady, Euler equations. The scheme, in strong conservation form, is based on a third-order upwind finite volume scheme and a second-order explicit Runge–Kutta scheme. For the description of the scheme and its applications, please see Refs. 5 and 6. Here, we only describe the treatment of the boundary conditions for the blowing/suction and porous surface walls.

The boundary condition of the transpiration velocity at either blowing/suction or porous surface walls is given as

$$\boldsymbol{u} \cdot \boldsymbol{n} = v_n \tag{2}$$

where $\boldsymbol{n}$ is the unit normal direction of the solid surface and directs into the interior of the airfoil. For a blowing/suction wall v_n is given. Whereas for a porous material, v_n is given by using Darcy's law[10]

$$v_n = \sigma \Delta p \tag{3}$$

The porosity factor σ is the porosity distribution function determined by the viscosity and the permeability of the porous medium, and Δp is given by

$$\Delta p = p_{\text{wall}} - p_{\text{cavity}} \tag{4}$$

Following the usual assumption[10,11] the pressure in the cavity p_{cavity} is uniform. Then let the net mass flow through the cavity of length L be zero; that is,

$$\int_L \rho v_n \, \mathrm{d}S = 0 \tag{5}$$

The pressure in the cavity can be evaluated by substituting Eqs. (3) and (4) into (5) and given by

$$p_{\text{cavity}} = \frac{\int_S \rho\sigma p_{\text{wall}} \, \mathrm{d}S}{\int_S \rho\sigma \, \mathrm{d}S} \tag{6}$$

As for the other parameters that are necessary for handling the wall boundary conditions, such as the tangential velocity, wall pressure, and wall density, they are calculated in the same way as that for a solid surface.

B. Kirchhoff Method

For the numerical assessment of BVI noise, a fine mesh system is necessary to precisely capture the acoustic perturbation. However, such a grid system will result in excessive CPU time and large memory storage requirements. Kirchhoff formulation is a convenient approach for the pressure field evaluation by means of information on a closed control surface in the midfield region. All of the nonlinear effects are assumed to be contained within the control surface. In the exterior of the surface, linear wave patterns are present. Therefore we only require fine mesh in the midfield domain and utilize the numerical solutions on the control surface as input to the Kirchhoff formula, to calculate the far-field value. Pierce[12] shows the formula for a fixed surface. The Kirchhoff formulation for an arbitrarily moving piecewise smooth deformable surface was derived by Farassat and Myers.[13]

Assume that all of the nonlinear effects and acoustic sources are present merely within a control surface S and three-dimensional waves propagate outward from the surface S. Although the numerical computations simulate two-dimensional parallel BVI problem, because of the assumption of high-blade aspect ratio the pressure of the three-dimensional BVI at the far-field region can be modeled from the Kirchhoff formulation. The pressure field outside the control surface S satisfies the wave equation

$$\nabla^2 p - \frac{1}{c_\infty^2}\left(\frac{\partial}{\partial t} + U_\infty \frac{\partial}{\partial x}\right)^2 p = 0 \tag{7}$$

where c_∞ and U_∞ are the ambient speed of sound and the freestream velocity, respectively. For fixed control surface S and utilizing the Prandtl–Glauert transformation

$$x_0 = x, \qquad y_0 = \beta y, \qquad z_0 = \beta z, \qquad r_0 = r_\beta \tag{8}$$

pressure outside the surface S is described as

$$p(x, y, z, t) = \frac{1}{4\pi}\int_S \left[-\frac{1}{r_0}\frac{\partial p}{\partial n_0} + \frac{1}{c_\infty r_0 \beta^2}\frac{\partial p}{\partial t} \times \left(\frac{\partial r_0}{\partial n_0} - M_\infty \frac{\partial x_{01}}{\partial n_0}\right) + \frac{p}{r_0^2}\frac{\partial r_0}{\partial n_0}\right]_\tau \mathrm{d}S_0 \tag{9}$$

where

$$r_\beta = \left\{(x - x_s)^2 + \beta^2\left[(y - y_s)^2 + (z - z_s)^2\right]\right\}^{\frac{1}{2}}$$

$$\tau = \left[r_\beta - M_\infty (x - x_s)\right] / c_\infty \beta^2$$

$$\beta = \left(1 - M_\infty^2\right)^{\frac{1}{2}} \tag{10}$$

M_∞ is the freestream Mach number and τ represents the time delay for wave to propagate from source (x_s, y_s, z_s) to observation position (x, y, z). The subscript 0 denotes the transformed value, τ denotes that all of the values are calculated at the retarded time $t_s = t - \tau$, and n is the outward normal direction of S. The preceding equations can be also found in Morino.[14,15]

Because of the high-aspect-ratio assumption, the strip theory is used in spanwise direction, and the two-dimensional numerical solution is accepted for every strip. The space enclosed by the control surface is expected to be large enough to contain all of the nonlinear effect, but, because of grid stretching, the numerical solutions may not be accurate enough on too large a surface. Therefore the appropriate selection of the position of the surface is essential. Because the contribution from the tip surface can be neglected,[2] the surface integration of Eq. (9) excludes tip-surface effects here. The aspect ratio is assumed to be 20, and 800 strips are used in the spanwise direction.

III. Numerical Tests

Three numerical tests are performed here to see the accuracy of the Kirchhoff method and MOC scheme.

A. Spherical Wave Test

A spherical pulse wave is assumed to radiate from a point source.[2] The amplitude of the wave is

$$p(r, t) = \begin{cases} \sin[(t - \tau)\pi / A] / r_\beta & \text{for} \quad 0 < t - \tau < A \\ 0 & \text{elsewhere} \end{cases}$$

where A is the wave thickness (or half period) and τ, r_β are given in Eq. (10) with $(x_0, y_0, z_0) = (0, 0, 0)$. In this test the Mach number is 0.822, and A is 1.1. To test the accuracy of the grid system used for the NACA0012 airfoil in BVI research, the airfoil grid of 120×190 and three integral surfaces shown in Fig. 1 are used in this test. The comparison of the theoretical solution and that solved using the Kirchhoff method with the integral surface S_3 at position $(-3, 0, 0)$ are shown in Fig. 2. The two solutions coincide with each other satisfactorily.

B. Porous Wall on NACA0012 Airfoil

A porous wall to modify flow phenomenon has been studied in Refs. 8–11. Generally in a transonic flow, a supersonic pocket occurs at the shoulder of airfoil, and the supersonic pocket is terminated by a normal shock wave. The flowfield is shown schematically in Fig. 3. The flow experiences a severe pressure jump across the shock

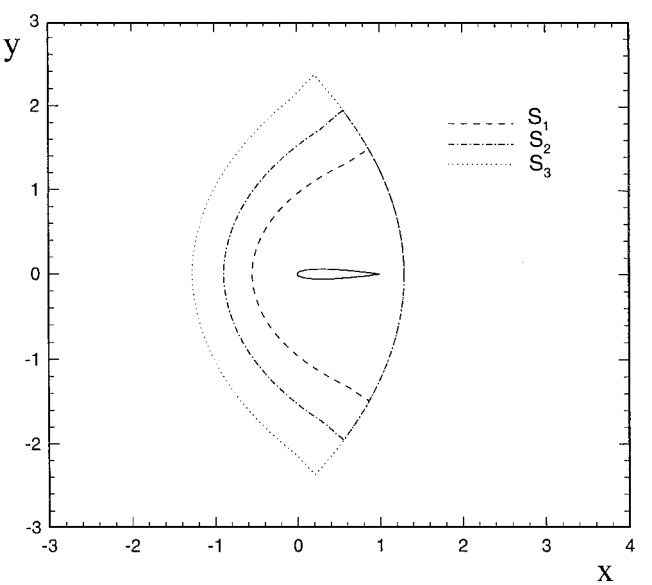

Fig. 1 Three chosen control surfaces for the Kirchhoff method.

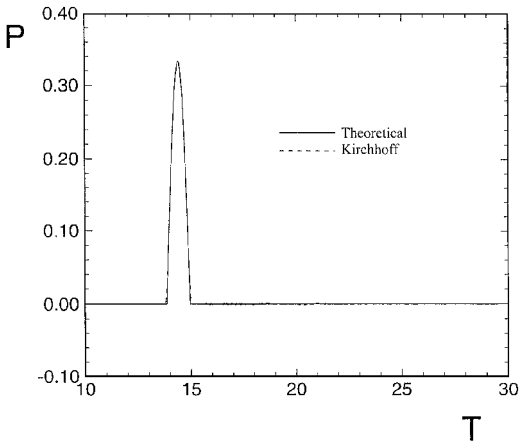

Fig. 2 Comparison of the theoretical solution and that solved from Kirchhoff method at position (− 3, 0, 0).

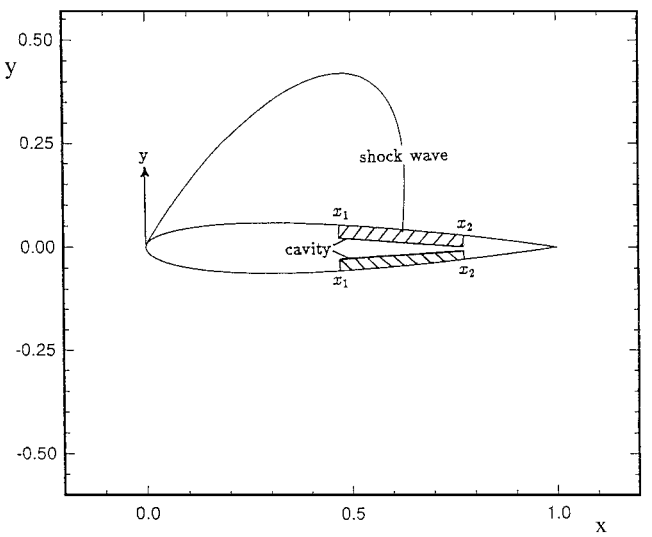

Fig. 3 Schematic for the porous airfoil on both lower and upper surfaces.

and thus leads to reduction of the aerodynamic performance. Downstream information cannot propagate upstream in a supersonic flow. But if a porous surface is employed at the position of shock's foot, the high pressure information can be propagated upstream through the porous cavity. Therefore, the shock strength can be weakened and controlled by porosity.

Here a NACA0012 airfoil with subcritical and supercritical flow speeds with a porous surface is evaluated. The freestream Mach number M_∞ is 0.63, and the angle of attack α is 2 deg for the subcritical flowfield, whereas for the supercritical flowfield $M_\infty = 0.8$ and $\alpha = 1.25$ deg. The porosity is distributed according to a squared root of a sine function:

$$\sigma = \sigma_{\max}\sqrt{\sin\left(\frac{x - x_1}{x_2 - x_1}\right)\pi} \tag{11}$$

where x_1 and x_2 are the two ends of the porous cavity as shown in Fig. 3. In this test the values of x_1 and x_2 for both upper and lower airfoil surface are 0 and 1, respectively. In other words the porous cavity is adopted along the entire chord in order to obtain the greatest modification of the surface-pressure distribution. The maximum porosity factor $\sigma_{\max}$ is taken to be 0.6. According to Eq. (11), there is zero porosity at the leading and trailing edges. Chen et al.[11] pointed out that this leads to the applicability of the assumption of a constant pressure in the cavity. Otherwise the cavity pressure should be solved simultaneously if this uniform pressure assumption is not suitable.

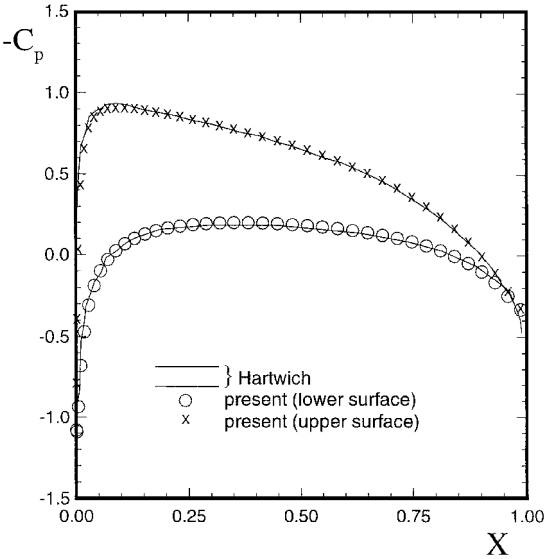

Fig. 4 Pressure coefficient of subcritical flow with M_∞ = 0.63, α = 2 deg.

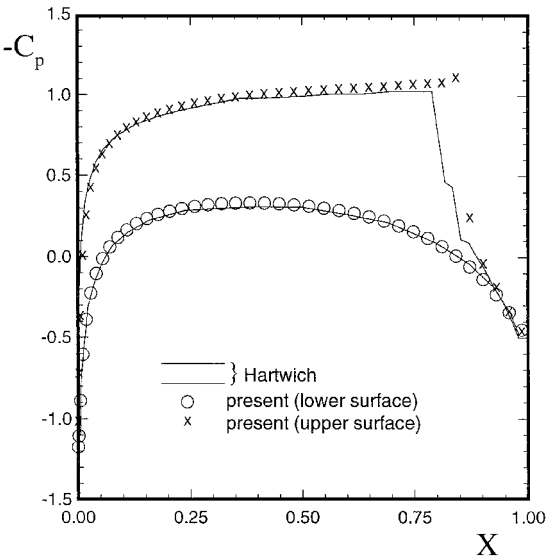

Fig. 5 Pressure coefficient of supercritical flow with M_∞ = 0.8, α = 1.25 deg.

The surface-pressure coefficient distribution is shown in Fig. 4 for the subcritical flow and in Fig. 5 for the supercritical flow. Comparison with results of Hartwich[8] are also included. There are small discrepancies except for the region near the shock wave. This difference near the shock location may be caused by the different shock capturing resolutions in two schemes. Hartwich used an in-house Euler solver, GAUSS2, which is a shock-fitting finite difference scheme. This is different from our shock-capturing finite volume scheme.

C. Noise Radiated by BVI

A vortex released upstream produces noise upon interaction with a blade. This blade vortex interaction is simulated in two dimensions using a NACA0012 airfoil. In a previous paper[5] authors applied the MOC scheme to investigate the flowfields and the phenomena of two dominant waves of BVI in detailed. The parametric study of BVI, the accuracy of the scheme, and grid independence were performed. Here we are mainly concerned with the far-field pressure fluctuation and the reduction of BVI noise. Let the oncoming flow Mach number M_∞ be 0.76 and the vortex strength Γ (defined by the maximum circulation divided by the freestream velocity and the chord length of the airfoil) be -0.3. At $t = 0$ the vortex is embedded

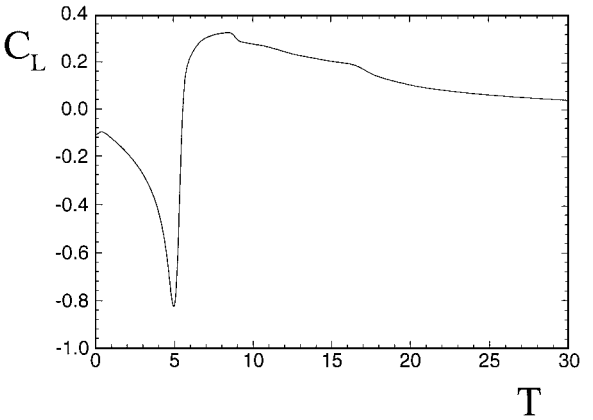

Fig. 6 Time variations of the lift C_L coefficient.

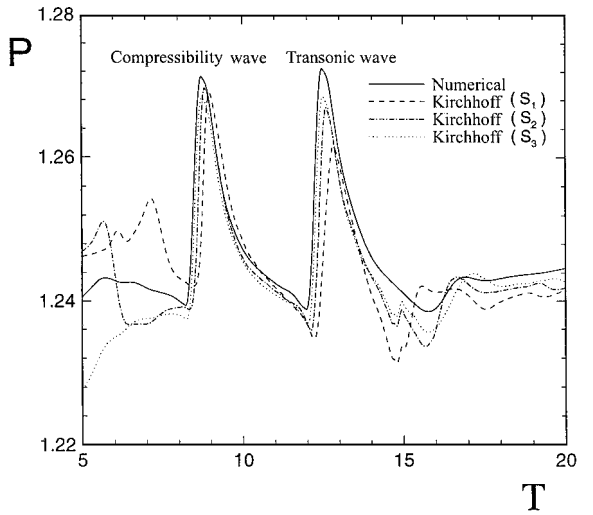

Fig. 7 Comparison of the pressure variation solved directly by the MOC scheme and that by the Kirchhoff method at $x = -1.4$, $y = 0$, $z = 0$.

at $x_0 = -5$ and $y_0 = -0.2$ (normalized by the chord length); afterwards it convects downstream. The time variation of the lift coefficient is shown in Fig. 6. Under the influence of the convecting vortex, the lift coefficient decreases before the vortex arrives at the airfoil leading edge and then increases after the vortex convects past the airfoil leading edge. Two waves radiate upstream resulting from the interaction of blade and vortex. The first wave, the compressibility wave, propagates outward during the vortex passing through the airfoil leading edge.[4,5] The second wave, the transonic wave, propagates upstream after the shock wave on the airfoil lower surface leaves the airfoil. Figure 7 is the comparison of the pressure variation at $x = -1.4$, $y = 0$, $z = 0$ as solved directly by the numerical method and by the Kirchhoff method. In this figure three control surfaces as shown in Fig. 1 are adopted for the calculations using the Kirchhoff formula, and tip surfaces are excluded in the calculations of the formula. For the compressibility wave the solutions with the three Kirchhoff surfaces are very similar to the numerical solution, whereas for the transonic wave solutions using control surface $S3$ match better with the numerical solution. Moreover, solutions using $S2$ and $S3$ have similar behavior with each other. Therefore $S3$ is large enough to contain all of the nonlinear effects inside it, and it is accepted for the following calculation.

Assume all waves radiate from the airfoil leading edge. Then if originally a wave radiates outward to (r, θ), influenced by uniform stream, the wave finally arrives (r_v, θ_v). The propagation graph is shown in Fig. 8. To inspect the radiation patterns of the waves, fix r_v, and observe the variation accompanied with angle variation. This is shown in Fig. 9 with $r_v = 50$. It is clear that the two waves radiate mainly to the upstream direction.

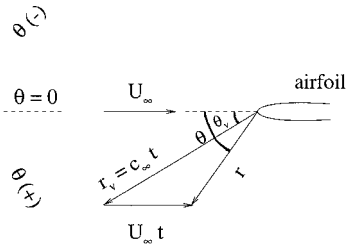

Fig. 8 Propagation graph for an airfoil-fixed coordinate system.

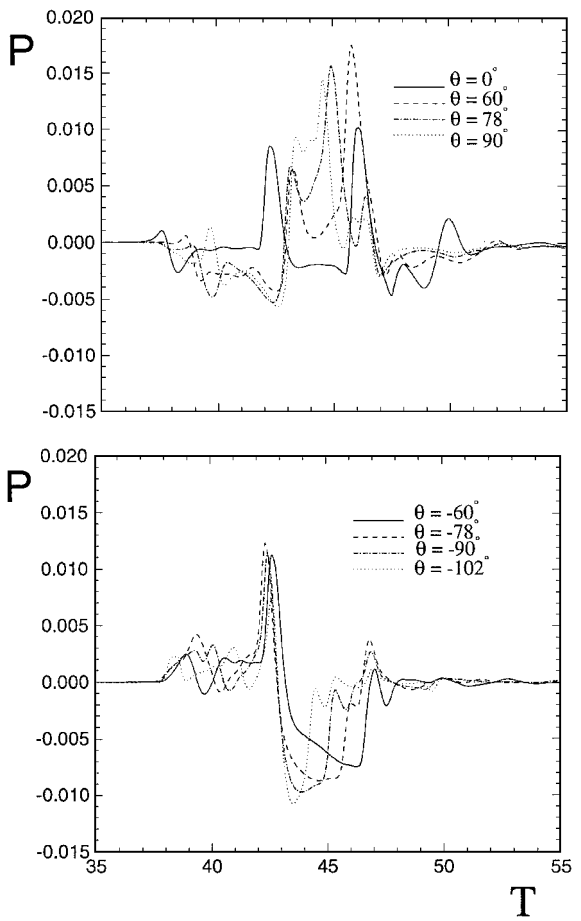

Fig. 9 BVI noise directivity for $M_\infty = 0.76, r_v = 50$.

IV. Noise Control by Blowing/Suction

In the study of Lin and Chin,[5] it was shown that the radiation of BVI noise is consistent with stagnation point motion and shock motion. As the vortex approaches the leading edge of the airfoil, the stagnation point moves, and the compressibility wave may be produced. Later the vortex approaches around the normal shock, and the shock begins to move. As the vortex passes through, the moving shock causes a severe pressure variation, and this is the mechanism responsible for transonic wave. This unsteady motion creates the unsteady force fluctuations that serve as the noise sources. A control law is designed in accordance with the characteristics of these noise sources in order to eliminate the strength of the compressibility and the transonic waves. Furthermore the reduction of the unsteady force fluctuations will simultaneously reduce the sound radiation.

In the acoustic far field the airfoil can be regarded as a point source, and the total integral of the pressure force on the airfoil corresponds to the lift force of the airfoil. So, the blowing/suction control law, which is used to control the injection volume flow, is based on the airfoil lift coefficient and is given by

$$Q = g \cdot C_l \tag{12}$$

where Q is the volume of flow injected from the blowing/suction region, C_l is the lift coefficient, and g is the gain of the control law.

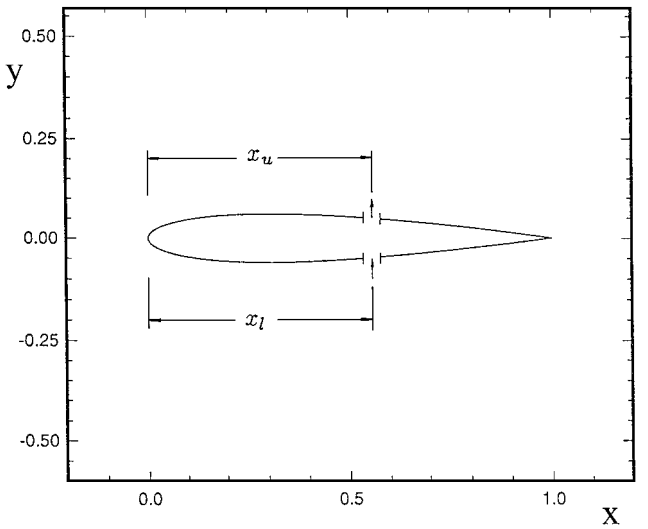

Fig. 10 Schematic for the blowing/suction control on the blade surface.

A positive value of Q represents blowing at the lower surface, and conversely a negative value of Q stands for suction at the lower surface. Figure 10 indicates the position where control is used on the airfoil surface with a negative value of Q. Here x_u and x_l are the positions where blowing/suction is employed on the upper and lower airfoil surface, respectively. Because an unsteady mass flux in the flowfield is equivalent to a monopole source, to prevent the participation of an extra noise source a symmetrical combination of blowing and suction is used. That is, when the blowing is employed at x_u on the upper surface, suction is used at x_l on the lower surface. Therefore, the total volume flow rate added for the control is zero. According to the no-penetration condition of a solid wall, the surface normal velocity is zero. However the injected volume flow at the blowing/suction region brings in a normal velocity. Therefore, to avoid high gradient distribution of normal velocity in the chordwise direction at two sides of the blowing/suction positions, let the blowing/suction source be located at a small region instead of a point. In our computations the blowing/suction volume flow is distributed over five mesh points, and the proportion of the volume flow distribution for the five meshes is 1:3:5:3:1.

Consider a flowfield with vortex strength $\Gamma = -0.3$, the oncoming flow Mach number $M_\infty = 0.76$, and the initial vortex position $x_0 = -5$, $y_0 = -0.2$. The lift coefficient history of the standard case is shown in the Fig. 6. The gain of the control law is designed as

$$g = \begin{cases} -0.04 & \text{if} \quad C_L < 0 \\ -0.05 & \text{if} \quad C_L > 0 \end{cases}$$

The design means that, when the lift coefficient is negative, blowing is applied at the lower surface and suction is applied at the upper surface. Conversely, if the lift coefficient is positive, the lower surface uses suction, and the upper surface uses blowing.

We fix the value of the gain for the control law and change the position of blowing/suction. Because of the symmetrical characteristics of the control position on the upper and lower surfaces, we set $x_u = x_l = x_c$. The history of the lift coefficient for four different control positions, $x_c = 0.3$, 0.5, 0.7, and 0.9, are shown in Fig. 11. When the flowfield is controlled by blowing and suction, the amplitude of the lift variation decreases no matter where the control technique is applied. Therefore, the design purpose is accomplished. For $x_c = 0.9$ the lift variation is the smallest among the four control locations. Figure 12 is the history of the volume flow magnitudes Q for the four control positions.

The decrease of the unsteady lift fluctuation in the flowfield may be one of the control targets. However, in this paper the reduction of the noise is the main subject. To understand the reduction of the acoustic noise, we compare the flowfield phenomenon of the four controlled cases with the standard uncontrolled flowfield. Figures 13a–13c show the pressure fluctuations history for $r_v = 50$

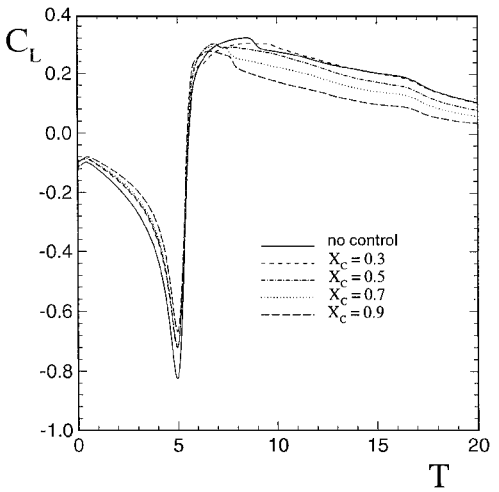

Fig. 11 Lift coefficient history for comparison of four control positions.

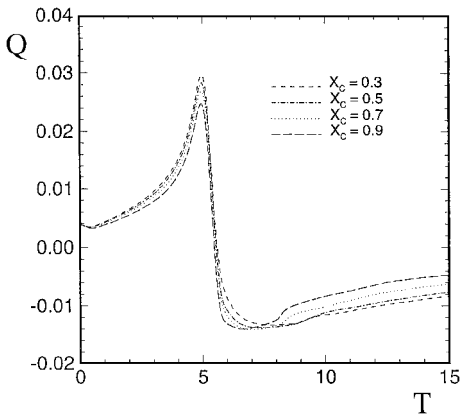

Fig. 12 History of the volume flow magnitudes Q for the four test control positions.

and $\theta = 60$, 0, and -78 deg, respectively. As shown in this figure, the compressibility wave is little influenced, whereas the reduction on the transonic wave is obvious. Because for the standard case the lower surface shock wave can only move backward to approximately 0.5 chord, the control positions $x_c = 0.7$ and 0.9 cannot directly modify the shock strength. Moreover they even prohibit the retreat motion of the lower surface shock and result in stronger shock strength. Therefore, as shown in Fig. 13, for $x_c = 0.7$ and 0.9 a transonic wave arrives at those positions more quickly than other cases, and the pressure disturbance is larger than the original standard disturbance value. However for $x_c = 0.3$ and 0.5 they situate within the route of the shock wave and can influence the shock strength directly. Besides, the uncontrolled shock wave has the strongest strength at 0.5 chord. Consequently the acoustic intensity for $x_c = 0.3$ and 0.5 should be expected to be smaller, and $x_c = 0.5$ possesses the most satisfactory results.

Because of little influence on the compressibility wave, it is expected that one should employ the blowing/suction technique at around the leading edge where the stagnation point travels around. Unfortunately, the present numerical simulation cannot sustain such leading-edge perturbation induced in combination by the blowing/suction and the blade-vortex interaction. We suspect that the combination will produce stronger interaction between the blade and the vortex. Therefore it is necessary to modify the blowing/suction simulation method, such as Navier–Stokes solvers, and this is a future subject to be investigated.

V. Noise Control by Using Porous Wall

Now we use the surface porosity to control the flowfield of the blade-vortex interaction problem. Two positions of the porous cavity are selected for comparison. The first is located at the airfoil leading

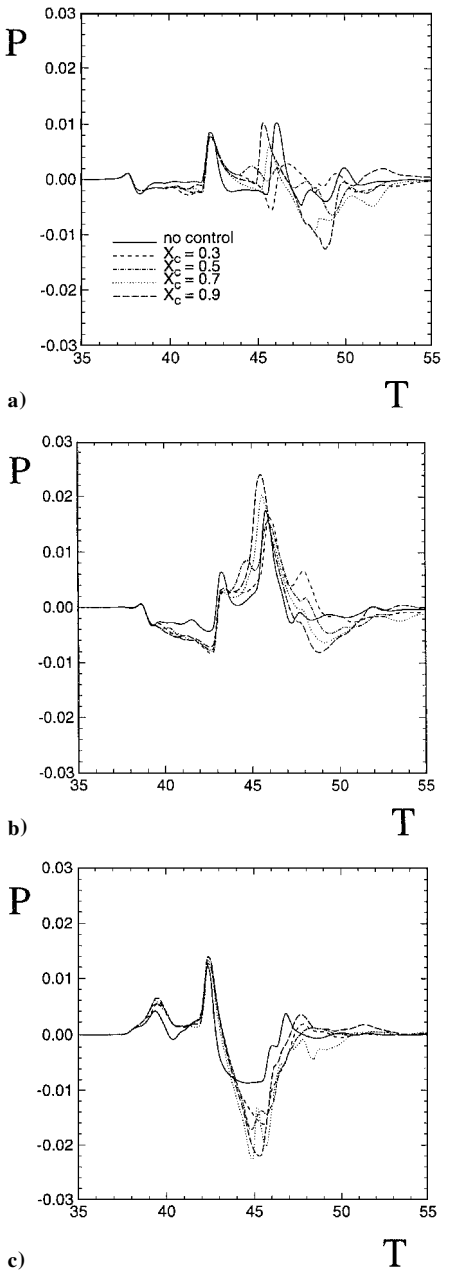

Fig. 13 Pressure fluctuations history at r_v = 50 and θ = a) 60 deg, b) 0 deg, and c) − 78 deg.

edge with $x_1 = 0$ and $x_2 = 0.2$, as indicated in Fig. 3. The second uses the maximum extension of the cavity and therefore set $x_1 = 0$ and $x_2 = 1.0$. The maximum porosity factor $\sigma_{\max}$ is 0.6. For symmetric concerning the porous surface is adopted on both the upper and lower surfaces with the same extent of cavity. The lift coefficient is shown in Fig. 14. Because the total lift of the airfoil is contributed primarily from the unsteady shock motion, the small porosity of the airfoil leading edge does not significantly affect the total integral value. As for the second case with $x_1 = 0$ and $x_2 = 1$, it has a larger lift force variation that resulted from the completely different flowfield affected by porosity.

Similarly, the pressure history is shown in Fig. 15 for $r_v = 50$ and $\theta = 60$, 0, and −78 deg. The compressibility and transonic wave are influenced obviously as recorded by the pressure history. This is different from the situation controlled by the blowing/suction because the blowing/suction is effective only when the shock wave travels across it while the porous wall modifies the flowfield around it especially for the case of $x_1 = 0$ and $x_2 = 1$. In Fig. 15, when $\theta = 0$ deg, the maximum peak of the transonic wave can be reduced about 84%, and the compressibility wave can be reduced 42% for

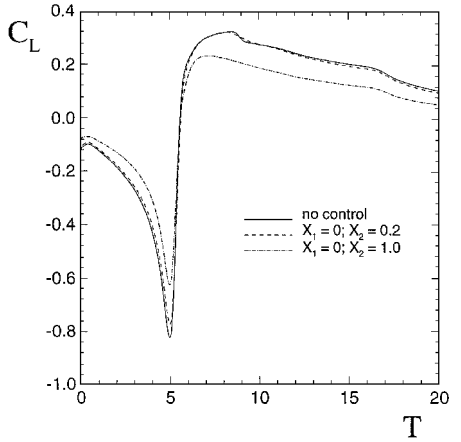

Fig. 14 Lift coefficient history for the porous surface.

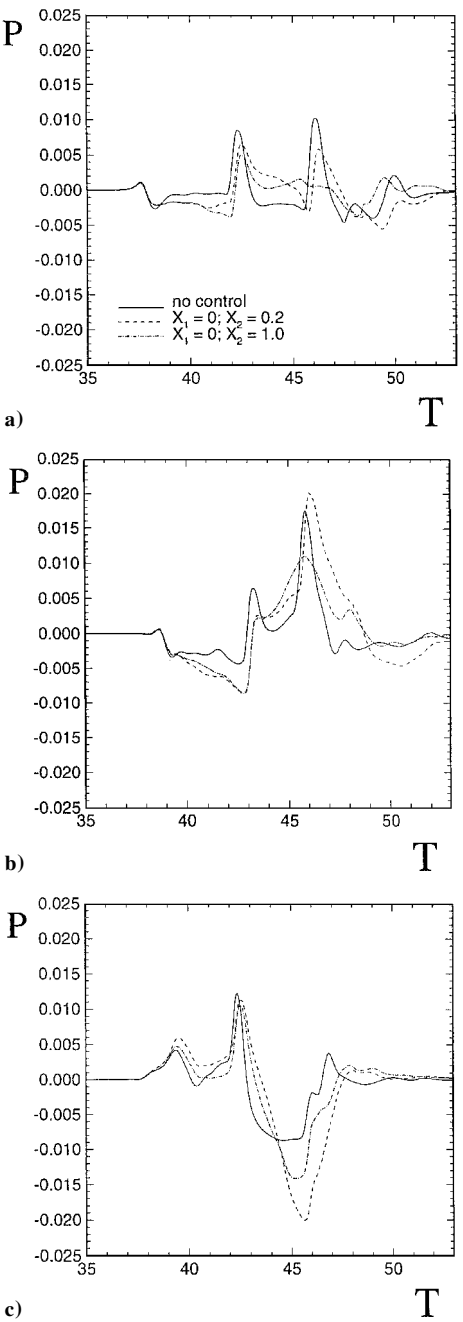

Fig. 15 Pressure fluctuations history for the porous surface at r_v = 50 and θ = a) 60 deg, b) 0 deg, and c) − 78 deg.

$x_1 = 0$ and $x_2 = 1$. For $\theta = 60$ deg, the transonic wave can be reduced about 37%, and for $\theta = -78$ deg the compressibility wave can be reduced about 15%.

The effect on the compressibility wave is smaller than that on the transonic wave. The possible reasons are 1) the porous surface is expected to decrease the pressure difference across shock through the communication in the porous cavity; 2) the porosity factor at the leading edge is zero; and 3) for the stagnation point movement there is no significant pressure variation experienced when the stagnation point passes through it. Because the compressibility wave mainly comes from the movement of the stagnation point, the modification for the compressibility wave is not as satisfactory as that for the transonic wave.

VI. Conclusion

The MOC scheme is applied to study the reduction of noise as a result of the transonic blade-vortex interaction. Two control techniques are used: the blowing/suction and porous wall on the airfoil surface. For the blowing/suction technique a control law is proposed in accordance with the lift coefficient to eliminate the strength of the compressibility and the transonic waves. Four control positions are chosen to employ the blowing/suction technique, and they are 0.3, 0.5, 0.7, and 0.9 chord length. Basically they are situated around the region where shock is present. Control on such a region can weaken the strength of shock that passes through it. The control technique reduces the fluctuations generated by the transonic wave and has little influence directly on the compressibility wave. Although shock locates close to 0.3 chord length initially, during the approach of vortex it is forced to move downstream near to 0.5 chord length with strength increasing simultaneously. Therefore the control position $x_c = 0.5$ has the most satisfactory results for reduction of the transonic wave. For the reduction of the compressibility wave, this control makes little contribution. We have tried to utilize the technique on the leading edge where the stagnation point travels around. But there are some numerical simulation difficulties for such a strong interaction problem that will be investigated in the future. As for the control by surface porosity, by examining the decrease of the pressure for both the compressibility and transonic wave the results are satisfactory. This indicates that the control by surface porosity is an efficient control technique for the reduction of noise caused by the transonic BVI.

Acknowledgment

This work is partially supported by the National Science Council of the Republic of China under Contract NSC86-2212-E006-105.

References

[1]Schmitz, F. H., and Yu, Y. H., "Helicopter Impulsive Noise: Theoretical and Experimental Status," *Recent Advance in Aeroacousitcs*, edited by A. Krothapalli and C. A. Smith, Springer-Verlag, New York, 1986, pp. 149–243.

[2]George, A. R., and Lyrintzis, A. S., "Acoustics of Transonic Blade-Vortex Interactions," *AIAA Journal*, Vol. 26, No. 7, 1988, pp. 769–776.

[3]Lee, S., Bershader, D., and Rai, M. M., "An Experimental and Computational Study of 2-D Parallel Blade-Vortex Interaction," AIAA Paper 91-3277, Sept. 1991.

[4]Lent, H. M., Meier, G. E. A., Muller, K. J., Obermeier, F., Schievelbusch, U., and Schurmann, O., "Mechanisms of Transonic Blade-Vortex Interaction Noise," *Journal of Aircraft*, Vol. 30, No. 1, 1993, pp. 88–93.

[5]Lin, S. Y., and Chin, Y. S., "Numerical Study of Transonic Blade-Vortex Interaction," *AIAA Journal*, Vol. 33, No. 8, 1995, pp. 1377–1382.

[6]Lin, S. Y., and Chin, Y. S., "Comparison of Higher Resolution Euler Schemes for Aeroacoustic Computations," *AIAA Journal*, Vol. 33, No. 2, 1995, pp. 237–245.

[7]Lyrintzis, A. S., and George, A. R., "Far-Field Noise of Transonic Blade-Vortex Interaction," *Journal of the American Helicopter Society*, Vol. 34, No. 3, 1989, pp. 30–39.

[8]Hartwich, P. M., "Euler Study on Porous Transonic Airfoil with a View Toward Multipoint Design," *Journal of Aircraft*, Vol. 30, No. 2, 1993, pp. 184–191.

[9]Lee, S., "Reduction of Blade-Vortex Interaction Noise Through Porous Leading Edge," *AIAA Journal*, Vol. 32, No. 3, 1994, pp. 480–488.

[10]Savu, G., and Trifu, O., "Porous Airfoils in Transonic Flow," *AIAA Journal*, Vol. 22, No. 7, 1984, pp. 989–991.

[11]Chen, C. L., Chow, C. Y., Holst, T. L., and Van Dalsem, W. R., "Numerical Simulation of Transonic Flow Over Porous Airfoil," AIAA Paper 85-5022, Oct. 1985.

[12]Pierce, A. D., *Acoustics: An Introduction to Its Physical Principles and Applications*, McGraw–Hill, New York, 1981, Chap. 5.

[13]Farassat, F., and Myers, M. K., "Extension of Kirchhoff Formula to Radiation from Moving Surfaces," *Journal of Sound and Vibration*, Vol. 123, No. 3, 1988, pp. 451–460.

[14]Morino, L., "A General Theory of Unsteady Compressible Potential Aerodynamics," NASA CR-2464, Dec. 1974.

[15]Morino, L., "Steady, Oscillatory, and Unsteady Subsonic and Supersonic Aerodynamics—Production Version 1.1 (SOUSSA-P, 1.1), Vol. 1, Theoretical Manual," NASA CR-159130, Jan. 1980.